Effective Passivation of Black Silicon Surfaces via Plasma-Enhanced Chemical Vapor Deposition Grown Conformal Hydrogenated Amorphous Silicon Layer

Özkol, Engin; Procel, Paul; Zhao, Yifeng; Mazzarella, Luana; Medlin, Rostislav; Šutta, Pavol; Isabella, Olindo; Zeman, Miro

DOI
10.1002/pssr.201900087

Publication date
2019

Document Version
Final published version

Published in
Physica Status Solidi - Rapid Research Letters

physica status solidi rrl
www.pss-rapid.com

Effective Passivation of Black Silicon Surfaces via Plasma-Enhanced Chemical Vapor Deposition Grown Conformal Hydrogenated Amorphous Silicon Layer

Engin Özkol, Paul Procel, Yifeng Zhao, Luana Mazzarella, Rostislav Medlin, Pavol Šutta, Olindo Isabella, and Miro Zeman*

Solar cells based on black silicon (b-Si) are proven to be promising in photovoltaics (PVs) by exceeding 22% efficiency. To reach high efficiencies with b-Si surfaces, the most crucial step is the effective surface passivation. Up to now, the highest effective minority carrier lifetimes are achieved with atomic layer-deposited Al_2O_3 or thermal SiO_2. Plasma-enhanced chemical vapor deposition (PECVD)-grown hydrogenated amorphous silicon (a-Si:H) passivation of b-Si is seldom reported due to conformality problems. In this current study, b-Si surfaces superposed on standard pyramidal textures, also known as modulated surface textures (MSTs), are successfully passivated by PECVD-grown conformal layers of a-Si:H. It is shown that under proper plasma-processing conditions, the effective minority carrier lifetimes of samples endowed with front MST and rear standard pyramidal textures can reach up to 2.3 ms. A route to the conformal growth is described and developed by transmission electron microscopic (TEM) images. Passivated MST samples exhibit less than 4% reflection in a wide spectral range from 430 to 1020 nm.

Black silicon (b-Si) refers to high-aspect ratio nano- and/or micro-textured features on silicon surface. This textured surface effectively suppresses reflection, thus the material appears black to the naked eye. The b-Si has several remarkable properties, such as low reflectance, large and chemically active surface area, and super-hydrophobicity.[1,2] Consequently, b-Si has a potential for a wide range of applications, such as self-cleaning surfaces,[3,4] microelectromechanical systems (MEMS),[5,6] chemical and bio-sensors,[7–9] drug analysis,[10,11] antibacterial surfaces,[12,13] and optoelectronic and photonic devices.[14–16]

Several fabrication techniques are employed for b-Si formation such as electrochemical etching,[17–19] stain etching,[20,21] metal-assisted chemical etching (MACE or MAE),[22–28] and reactive-ion etching (RIE).[29–31] Among these techniques, RIE has the advantages of fast and maskless processing, independency of crystalline orientation, and cost efficiency.[32]

The b-Si has been recently proven as an excellent surface functionalization of crystalline silicon (c-Si) material for photovoltaic (PV) technology in both front/back-contacted (FBC)[25] and interdigitated back-contacted (IBC)[33] architectures, enabling conversion efficiency beyond 22% in both mono[34] and multi-c-Si.[35] The b-Si has the potential to reduce the reflection to even below 1%,[36] while enhancing the scattering and absorption of light when combined with microscale surface features, such as the standard pyramidal texture.[33,37] It overall acts as a multi-anti-reflection coating (MARC) by smoothly matching the refractive index of c-Si with that of the incident medium (e.g., air).[38] As there is no need for an ARC layer, the b-Si may reduce the manufacturing cost of solar cells. However, the etching of silicon surface enhances the surface recombination velocity (SRV) and possibly lowers the bulk lifetime by increasing the surface area and introducing defects during b-Si fabrication process. Therefore, effective passivation of b-Si structures is the key issue to overcome this drawback.

Up to now, three of the four most common passivation materials employed in c-Si PV technology have been reported to passivate b-Si surfaces: SiN_x,[39,40] SiO_2,[41,42] and Al_2O_3,[43,44] or their combinations.[45,46] The usage of the fourth material, hydrogenated amorphous silicon (a-Si:H), is recently being investigated, albeit so far only applied on MAE[47] and cryogenic RIE-based b-Si,[48] successfully. Liu et al.[22] demonstrated the conformality issue of SiN_x layer deposited by plasma-enhanced chemical vapor deposition (PECVD) on b-Si surface and put forward a SiO_2/SiN_x stack for passivation. Khandelwal et al.[49] reported an effective lifetime of 1092 μs with thermal SiO_2 passivation layer and flat-passivated

Dr. E. Özkol,[+] Dr. P. Procel, Y. Zhao, Dr. L. Mazzarella, Dr. O. Isabella, Prof. M. Zeman
PVMD
Delft University of Technology
Mekelweg 4, Delft 2628 CD, The Netherlands
E-mail: engin.ozkol@gmail.com, engin.oezkol@helmholtz-berlin.de

Dr. R. Medlin, Dr. P. Šutta
New Technologies—Research Centre
University of West Bohemia
Pilsen CZ-30614, Czech Republic

The ORCID identification number(s) for the author(s) of this article can be found under https://doi.org/10.1002/pssr.201900087.

[+]Present address: Helmholtz-Zentrum Berlin fur Materialien und Energie GmbH, The Institute Silicon Photovoltaics, Kekuléstraße 5, 12489 Berlin, Germany

DOI: 10.1002/pssr.201900087

rear side. Otto et al.[50] reached 1475 µs lifetime on "intermediate" aspect ratio (about 4) b-Si surfaces passivated by Al_2O_3. Repo et al.[36] showed that with atomic layer deposition (ALD)-deposited Al_2O_3, the effective lifetime of minority carriers is in the order of milliseconds. Recently, transition metal oxides such as TiO_2,[51] Al_2O_3/TiO_2 stack,[52] and HfO_2[53] are reported to be promising passivation materials for b-Si surfaces.

In this work, b-Si surfaces superposed on standard microscale pyramidal textures (hereinafter referred as "modulated surface texture," MST) are passivated by low-temperature conformal layers of a-Si:H grown by means of PECVD technique. Although a-Si:H exhibits strong parasitic absorption, it is reported that the carrier injection efficiency of a-Si:H to c-Si is 100%,[54] which makes it a strong candidate for surface passivation. It is shown that the effective minority carrier lifetimes of the MST samples can reach values in the millisecond range. Methodology and results reported in this contribution enable the deployment of the b-Si as front surface functionalization in high-efficiency FBC and IBC c-Si solar cells manufactured at low thermal budget, such as those architecture based on heterojunction technology.

MST surfaces were fabricated by superposing dry-etched nanotexture (b-Si) on wet-etched microtextures (standard pyramids). To passivate the MST surfaces, a-Si:H layers were deposited via PECVD under several plasma conditions. Scanning electron microscopy (SEM) images taken at a tilt angle of 45° are reported in **Figure 1**, showing the morphology of the passivated samples for multiple magnifications. Both micro and nanotextures can be distinguished from lower magnification. High aspect ratio of MST structure can be visualized from the magnified area of SEM image.

The 50 nm thick a-Si:H films were deposited on MST samples to passivate the surfaces. The a-Si:H layer was deposited under 13 mW cm^{-2}, 0.7 mbar, 180 °C, and hydrogen to silane dilution ratio ($R = [H_2]/[SiH_4]$) of 3. In **Figure 2**, the reflectance of bare and SiN_x-coated microtextures as well as bare MST and a-Si:H-passivated MST is plotted. The optical impact of MST, when compared with only microtextures for all wavelength spectrum, is obvious, reducing the reflection to less than 4% in the wavelength range between 430 and 1020 nm. In the magnified inset figure, the reflection spectra of SiN_x-coated microtextures as well as bare MST and a-Si:H-passivated MST are plotted. Although SiN_x-coated microtextures show—as expected—anti-reflection effect in the wavelength range between 480 and 650 nm, the MST-based textures exhibit less than 4% reflection. In contrast, in the range of

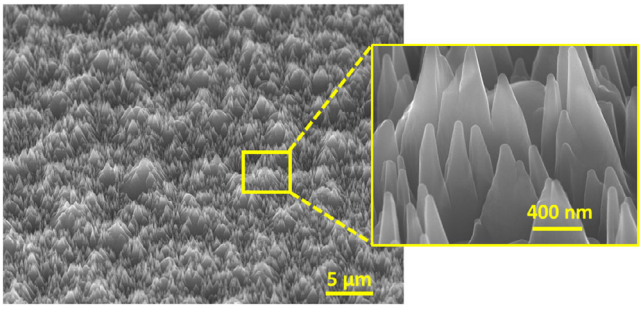

Figure 1. SEM images (45° tilted) of our typical MST front texture: (left) large area view, depicting the superposition of nano on microtextures and (right) zoom on the high aspect ratio features (b-Si) of the MST structure.

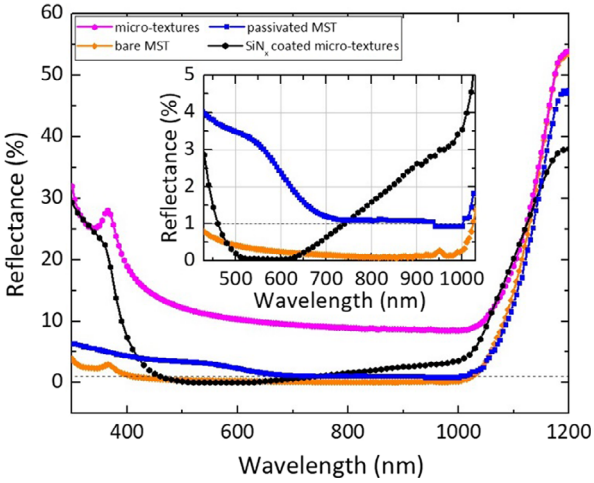

Figure 2. Reflectance spectra of bare and SiN_x-coated microtextures alongside bare and a-Si:H-passivated MST (under deposition conditions of 13 mW cm^{-2}, 0.7 mbar, 180 °C, and $R = 3$). The inset zooms in the spectral region where the reflectance is the lowest.

750–1020 nm, both MST samples show superior and broadband optical properties when compared with SiN_x-coated microtextures.

In chemical vapor deposition (CVD) processes, there are two main mechanisms that determine the film deposition rate: 1) mass transport and 2) surface reaction. To maintain conformal growth on complex and high aspect ratio structures such as MST, surface reaction should be suppressed with respect to mass transport. Otherwise, the film growth starts at the tips of the needle-like structure and the radicals cannot be transported inside valleys. As a result, film growth leaves voids in the valleys. This issue is demonstrated by Liu et al. and defined as "naked silicon surface."[22] To overcome void formation beneath the passivation layer, surface reaction should be limited to a minimum. The surface reaction flux depends strongly on surface temperature, whereas the temperature dependency of mass transport flux can be considered to be negligible.[55] Therefore, surface temperature is the key point for conformal growth.

To minimize the surface reaction rate and thus obtain denser films, temperature of the surface and the radical temperature in the plasma state should be kept as low as possible. In PECVD systems, this can be practically controlled by working under low-power regimes and/or reducing the substrate temperature. Next to that, to achieve high-quality surface passivation, the plasma gaseous composition has to be taken into consideration.

In our experiments, applied RF power density was kept constant at 13 mW cm^{-2}. This power is the minimum value for stable plasma conditions and uniform film deposition at a moderate pressure of 0.7 mbar and constant electrode distance of 10 mm in our PECVD chamber. Reducing the power even more resulted in nonuniformly distributed and unstable glow discharges. Although the deposition rates are low, setting such minimum power conditions, the deposited films are more defect-free (i.e., less voids) as expected from Paschen's curve of silane glow discharge.[56] Paschen's law simply defines the breakdown voltage of a gaseous mixture as a function of electrode distance (d) and pressure (p). It was observed that for low $p{\cdot}d$ product and power

region, more SiH_3 radicals are produced in silane discharge,[57] whereas at higher $p{\cdot}d$ product and power regions, SiH_2 and SiH radical formation is enhanced. As a result, under this minimum process parameter conditions, the probability of SiH_3 radical formation is greatly enhanced with respect to SiH_2 and SiH radical formation, leading to fine passivation of silicon surfaces.[58,59]

One of the most crucial parameters in a-Si:H passivation is the hydrogen dilution in the gas mixture.[60–63] It is known that the H atoms and SiH_3 radicals play an important role in plasma chemistry, thus the passivation.[60,64] Thus, it is crucial to determine the optimum hydrogen to silane dilution ratio ($R = [H_2]/[SiH_4]$). It was observed that R values higher than 5 may cause epitaxial growth.[65] This epitaxial growth circumstance should be avoided as it is detrimental for surface passivation quality.[66] Thus, the dilution ratio range was selected to be between 0 and 5. The effect of dilution ratio on the effective lifetime is illustrated in **Figure 3**. It is clearly seen that for the fixed plasma conditions of 13 mW cm^{-2}, 0.7 mbar and 180 °C, the best passivation is observed for a dilution ratio $R = 3$, yielding $\tau_{eff} = 2.2$ ms with an i-Voc around 720 mV. To have a better understanding of passivation quality of the MST side of the wafer, front (MST) SRVs are calculated according to Equation (1)[33]

$$\tau_{eff} \approx \frac{d}{S_{eff}^{B} + S_{eff}^{F}} + \frac{1}{D}\left(\frac{2d}{\pi}\right)^2 \quad (1)$$

where d is the wafer thickness, D is the diffusion constant of the excess carriers, and S_{eff}^{B} is the back and S_{eff}^{F} is the front (MST) SRV. S_{eff}^{B} is determined by Equation (2) from symmetrical a-Si:H deposition on double side textured (i.e., no MST) wafers.

$$S_{eff}^{B} \approx \frac{d}{2\tau_{eff}} \quad (2)$$

The effective minority carrier lifetimes at an injection level of 1×10^{15} cm^{-3} and calculated back (DST) and front (MST) surface recombination values are listed in **Table 1** with respect to silane to hydrogen dilution ratio. The lowest SRV of MST surface S_{eff}^{F} is 9.4 cm s^{-1} obtained at a dilution ratio of 3.

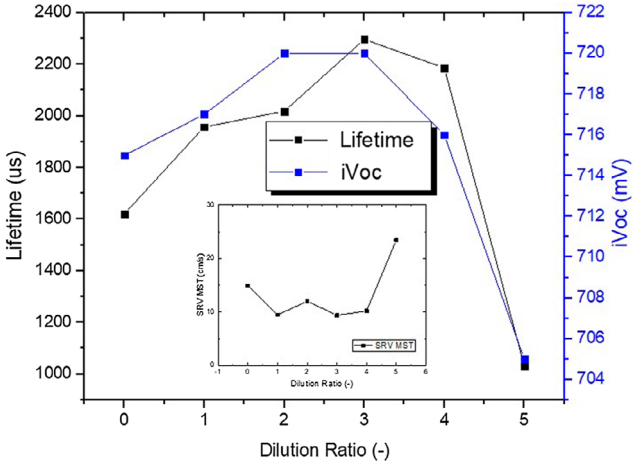

Figure 3. Influence of hydrogen dilution $R = [H_2]/[SiH_4]$ during PECVD of a-Si:H on effective minority carrier lifetimes and SRVs of MST samples (under fixed deposition conditions of 13 mW cm^{-2}, 0.7 mbar, and 180 °C).

Table 1. The effective minority carrier lifetimes and calculated back (Equation (2)) and front (Equation (1)) SRVs under several hydrogen dilution ratio and surface temperature values. Optical constant and dopant density used for the lifetime measurements are 1 and 1×10^{15} atoms cm^{-3}.

Variable		τ_{eff} DST [μs]	S_{eff}^{B} [cm s^{-1}]	τ_{eff} MST [μs]	S_{eff}^{F} [cm s^{-1}]
$R = [H_2]/[SiH_4]$	0	7778	1.74	1620	14.96
	1	3114	4.34	1957	9.48
	2	9773	1.38	2018	12.01
	3	5670	2.38	2296	9.39
	4	6263	2.16	2186	10.21
	5	4856	2.78	1032	23.45
Temperature [°C]	120	444	30.58	263	73.09
	140	668	20.29	470	37.47
	160	5737	2.35	1978	11.31
	180	5670	2.38	2296	9.39
	200	6470	2.09	2057	11.05

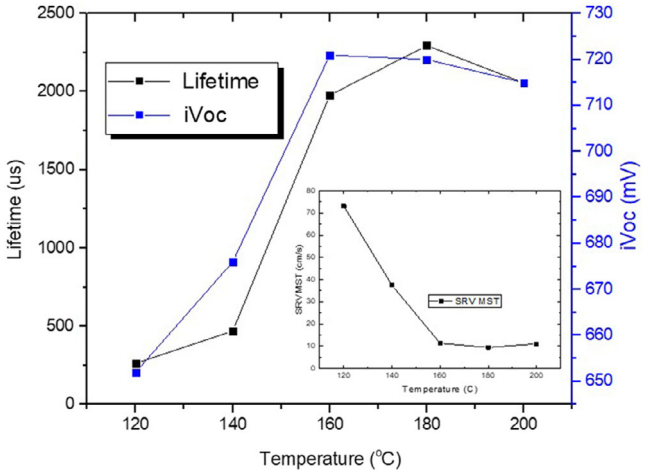

Figure 4. Influence of deposition substrate temperature on effective minority carrier lifetimes and SRVs of MST samples. Lower surface temperature corresponds to lower deposition substrate temperature. (Under fixed deposition conditions of 13 mW cm^{-2}, 0.7 mbar and $R = 3$.)

To further reduce surface reaction rate, substrate temperature should be lowered. Therefore, substrate temperature was reduced down to 120 °C as a proof of concept. In **Figure 4**, the effect of the surface temperature on surface passivation can be visualized. Reducing the temperature limits the surface reaction rate; however, at low surface temperatures, SiH_3 and hydrogen mobility are hindered in the deposited film. Thus, it is observed that the passivation quality gets lower for temperatures lower than 160 °C. Exceeding this temperature, the calculated SRV of MST (S_{eff}^{F}) reaches similar values that are lower than 11.4 cm s^{-1}. The minimum SRV and highest effective lifetime observed under the surface temperature of 180 °C are 9.4 cm s^{-1} and around 2.3 ms, respectively. In Table 1, τ_{eff} and calculated back (DST) and front (MST) surface recombination values according to various surface temperatures are listed.

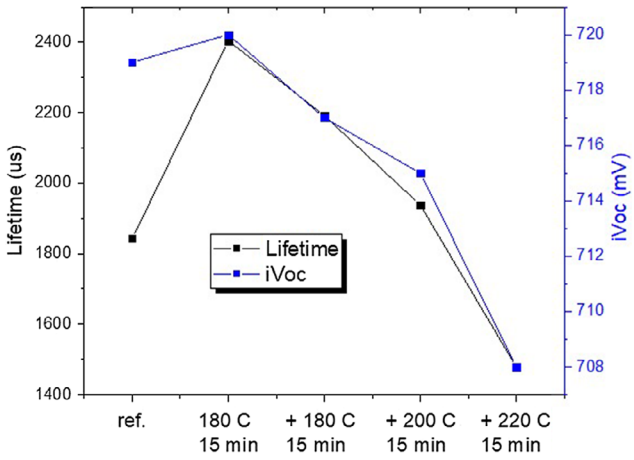

Figure 5. Influence of post-annealing of the sample that has the highest effective minority carrier lifetime under hydrogen atmosphere for several temperatures and duration. (Deposition conditions of 13 mW cm^{-2}, 0.7 mbar, 180 °C, and $R = 3$.)

In most of the silicon heterojunction (SHJ) solar cell fabrication processes, the required temperature is around or slightly below 200 °C. Therefore, a post-annealing study was also conducted and the results are shown in **Figure 5**. Before the annealing step, samples were kept under air atmosphere for 1 week. This period caused a degradation of lifetime from 2.2 to 1.8 ms. Nevertheless, annealing the samples at deposition temperature (180 °C) under Hydrogen flow in our PECVD chamber for 15 min has recovered the passivation quality and furthermore slightly increased the effective lifetime to 2.4 ms. However, increasing the annealing duration to 30 min at deposition temperature or annealing at higher temperatures had detrimental effects on passivation quality.

To investigate the conformality and the thickness of the deposited a-Si:H film on MST samples, transmission electron microscopic (TEM) analysis was performed. In **Figure 6**, TEM images of the samples that have been deposited at 120, 180, and 200 °C are shown. It is clearly seen that there is no conformality issue of PECVD-grown a-Si:H layer deposited at 120 °C. No void formation beneath the a-Si:H layers is observed from Figure 6a,b. The average thickness of the a-Si:H film is determined to be 45.5 ± 10 nm on the surfaces of the textures, and 55 ± 10 nm at the "valleys" and "peaks". We speculate that the thickness disuniformity arises from the variant resident times of the molecules inside such a complex structure. In other words, the radicals that are on the surfaces can be pumped away smoothly, whereas the radicals that are transported inside the nanovalleys are "trapped." Therefore, the surface concentration of the molecules inside the cavities increases. This accumulation leads in higher surface reaction rates and thus thicker films, as explained by mass transfer basics. Therefore, to obtain higher conformality, the balance between mass transport and surface reaction rate has to be adjusted in favor of surface reaction mechanism.

In Figure 6c,d, we observed the formation of bright areas between a-Si:H when the surface temperature is above 180 °C. This bright area is attributed to a void formation inside the passivation layer. This voids can be clearly seen in Figure 6e,f at which the surface temperature is risen up to 200 °C. At moderately high temperatures (i.e., 200 °C), the mass transport of molecules to the "valleys" is suppressed by surface reaction at the tip of the nanotextures. This phenomena leads to merging of the adjoining films growing at the tips of the textures and leaving a void beneath. Although these voids leave no "naked silicon surfaces," they will be an issue considering especially FBC-stacked SHJ structures. To overcome the void formation, surface reaction should be controlled precisely for high aspect ratio structures or thinner a-Si:H films (which is essential for high-efficiency SHJ solar cells) should be deposited for similar aspect ratio structures as in this study.

As a result, a trade-off between enhanced passivation and conformal growth for high aspect ratio structures is demonstrated.

In this contribution, modulated surface-textured samples (b-Si on microscale pyramids) exhibit less than 4% reflection in a wide

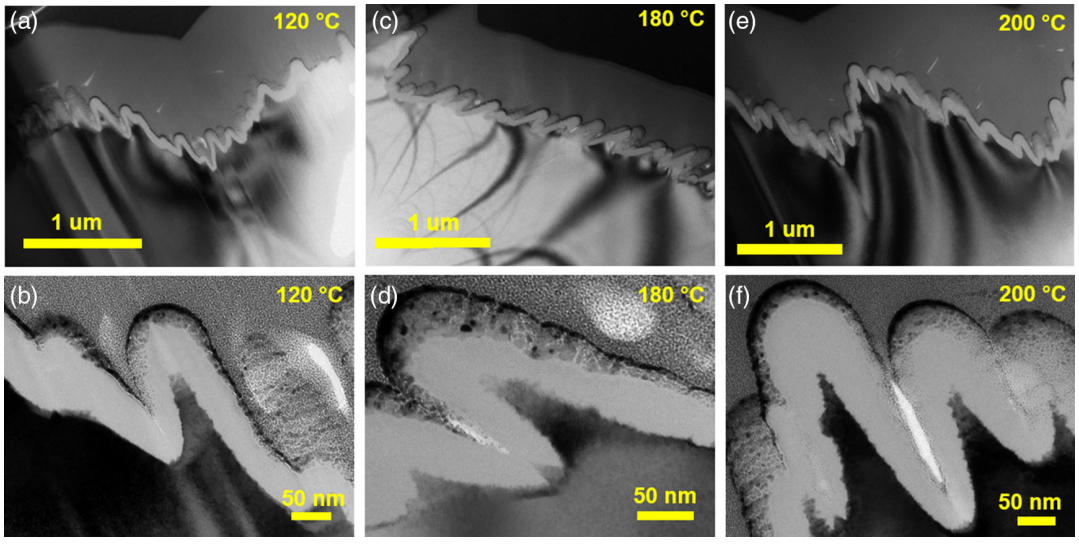

Figure 6. TEM images of a-Si:H films deposited on MST samples (Under deposition conditions of 13 mW cm^{-2}, 0.7 mbar and $R = 3$): a,b) Conformal growth under 120 °C. c,d) Initiation of the gap in the film at 180 °C. e,f) Formed gap between the film at 200 °C.

spectral range from 430 to 1020 nm. The MST samples are passivated by PECVD-grown a-Si:H layers. Plasma-processing conditions are tuned according to mass transfer basics, Paschen's curve basics, and SiH_3 radical formation kinetics. Before conducting gas flow ratio and temperature optimizations, the applied RF power density and deposition pressure are fixed to 13 mW cm^{-2} and 0.7 mbar, respectively. The desired hydrogen-to-silane dilution ratio is found to be 3 under this plasma regime to obtain good passivation. At the substrate temperature of 180 °C, the highest effective minority carrier lifetime of 2.3 ms is achieved. The conformality issue and void formation of PECVD technique for high aspect ratio structures at moderately high temperatures (around 200 °C) are observed and demonstrated by TEM images. A route to overcome conformality issue is described based on mass transfer basics. A trade-off between conformal growth and enhanced surface passivation for high aspect ratio textures is demonstrated.

Experimental Section

Double-side polished, n-type, <100> oriented, 4 in. wide float zone c-Si wafers with a thickness of 280 ± 20 µm and a resistivity of 1–5 Ω cm were used in this study. First, standard microscale texturing was performed with tetramethylammonium hydroxide (TMAH) solution on both sides of the wafers. Formation of b-Si on one side of the wafer was performed via a Drytek RIE equipment with SF_6 and O_2 gas mixture. After defect removal etching (DRE) and cleaning processes, so-called MST samples were obtained. The MST samples used in this work are visualized in **Figure 7**. Details about texturing, RIE, DRE, and cleaning processes can be found elsewhere.[33,67] The reflectance of the samples was measured by a Perkin Elmer Lambda 950 spectrophotometer.

RF-driven PECVD system with an electrode distance of 10 mm was used to deposit 50 nm thick a-Si:H layers. Thickness measurements were conducted by a Woollam EC-400 spectroscopic ellipsometer (SE) on films deposited on flat Corning Eagle XG glass substrates. The enlargement area factor, which is the ratio between the effective area of textured surface to the projected area on a flat surface, of MST surface is taken as 7 while adjusting the film thickness on MST surfaces for the passivation tests. This numerical factor is based on the enlargement factor of b-Si on flat interface[33] (≈4) multiplied by 1.7, as representative of the enlargement factor of standard pyramidal texture. To optimize the passivation, the effects of hydrogen-to-silane volumetric flow rate ratio (R) and substrate temperature were investigated during the experiments. Applied RF power density was kept at the minimum uniform plasma ignition value of 13 mW cm^{-2}, according to preliminary results. The deposition pressure and total flow rate of the gas mixture are fixed at 0.7 mbar and 40 sccm, respectively. Under these fixed parameters and constant electrode distance, the thickness uniformity is preserved for an area of 100 cm^2. For high- and low-pressure regimes (at constant electrode distance), the thickness uniformity is lost as explained by Paschen's curve. Mass transfer basics, Paschen's curve, and SiH_3 radical formation kinetics were taken into consideration for this study. The deposition parameters are tabulated in **Table 2**.

To determine the morphology of the MST surface, JEOL JSM-7600F SEM was used. Thickness and conformality of the deposited films were determined by high-resolution transmission electron microscopy (HRTEM). Sinton Consulting WTC-120 photoconductance decay lifetime tester was used to measure the effective lifetime (τ_{eff}) of the passivated samples in transient mode at an injection level of 1×10^{15} cm^{-3}.

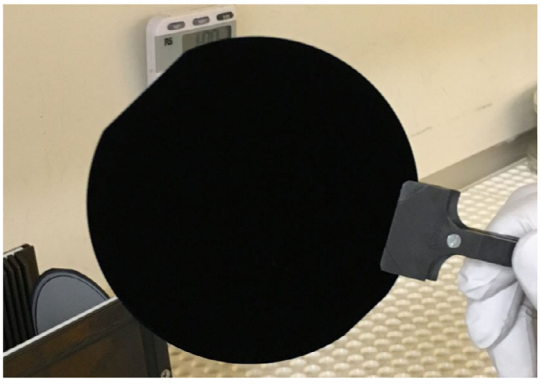

Figure 7. The MST samples after RIE and DRE steps.

Table 2. PECVD deposition conditions of a-Si:H layers. $R = [H_2]/[SiH_4]$ is the hydrogen-to-silane ratio.

Parameter	Value	Unit
Pressure	0.7 (fixed)	mbar
Total flow rate	40 (fixed)	sccm
RF power density	13 (fixed)	mW cm^{-2}
Hydrogen dilution [R]	0-1-2-3-4-5	–
Substrate temperature	120-140-160-180-200	°C
Deposition time	56:02-26:11-21:28-22:00-25:50-32:04[a)] 22:00-26:06-22:00-22:00-25:18[b)]	min:s

[a)]Deposition times with respect to ascending dilution ratio; [b)]Deposition times with respect to ascending substrate temperature.

Acknowledgements

E.Ö. acknowledges financial support from the Scientific and Technological Research Council of Turkey (TUBITAK) BIDEB-2219 Postdoctoral Research Programme. Results were also developed within 1) the CENTEM project, reg. no. CZ.1.05/2.1.00/03.0088, co-funded by the ERDF as part of the Ministry of Education, Youth and Sports OP RDI programme; 2) the follow-up sustainability stage, supported through CENTEM+ (LO1402) by financial means from the Ministry of Education, Youth and Sports under the "National Sustainability Programme I."; and 3) in the framework of NextBase project, that has received funding from the European Union's Horizon2020 Programme for Research, Technological Development and Demonstration under Grant agreement no. 727523. The authors also acknowledge Dr. Guangtao Yang from the Photovoltaic Materials and Devices group of Delft University of Technology for providing with one of the reference reflectance spectra.

Conflict of Interest

The authors declare no conflict of interest.

Keywords

black silicon, conformal growth, hydrogenated amorphous silicon, plasma-enhanced chemical vapor deposition, surface passivation

Received: February 12, 2019
Revised: September 20, 2019
Published online: October 24, 2019

[1] X. Liu, P. R. Coxon, M. Peters, B. Hoex, J. M. Cole, D. J. Fray, *Energy Environ. Sci.* **2014**, *7*, 3223.

[2] V. Zorba, L. Persano, D. Pisignano, A. Athanassiou, E. Stratakis, R. Cingolani, P. Tzanetakis, C. Fotakis, *Nanotechnology* **2006**, *17*, 3234.
[3] J. Zhu, C.-M. Hsu, Z. Yu, S. Fan, Y. Cui, *Nano Lett.* **2010**, *10*, 1979.
[4] Y. Zeng, X. Fan, J. Chen, S. He, Z. Yi, X. Ye, Y. Yi, *Superlattices Microstruct.* **2018**, *117*, 144.
[5] M. J. D. Boer, J. G. E. (H.) Gardeniers, H. V. Jansen, E. Smulders, M.-J. Gilde, G. Roelofs, J. N. Sasserath, M. Elwenspoek, *J. Micromech. Microeng.* **2002**, *11*, 385.
[6] W. Liu, A. Ming, Y. Ren, Q. Tan, W. Ou, X. Sun, W. Wang, D. Chen, J. Xiong, in *Proc. of IEEE 11th Annual Int. Conf. on Nano/Micro Engineered and Molecular Systems*, IEEE, Sendai **2016**.
[7] A. Jane, R. Dronov, A. Hodges, N. H. Voelcker, *Trends Biotechnol.* **2009**, *27*, 230.
[8] L. D. Stefano, L. Moretti, A. Lamberti, O. Longo, M. Rocchia, A. M. Rossi, P. Arcari, I. Rendina, *IEEE Trans. Nanotechnol.* **2004**, *3*, 49.
[9] D. P. Tran, T. T. T. Pham, B. Wolfrum, A. Offenhäusser, B. Thierry, *Materials* **2018**, *11*, 785.
[10] L. Sainiemi, H. Keskinen, M. Aromaa, L. Luosujarvi, K. Grigoras, T. Kotiaho, J. M. Makela, S. Franssila, *Nanotechnology* **2007**, *18*, 505303.
[11] W. Xu, K. Tamarov, L. Fan, S. Granroth, J. Rantanen, T. Nissinen, S. Peräniemi, O. Uski, M.-R. Hirvonen, V.-P. Lehto, *ACS Appl. Mater. Interfaces* **2018**, *10*, 23529.
[12] E. P. Ivanova, J. Hasan, H. K. Webb, G. Gervinskas, S. Juodkazis, V. K. Truong, A. H. F. Wu, R. N. Lamb, V. A. Baulin, G. S. Watson, J. A. Watson, D. E. Mainwaring, R. J. Crawford, *Nat. Commun.* **2013**, *4*, 2838.
[13] G. Hazell, P. W. May, P. Taylor, A. H. Nobbs, C. C. Welch, B. Su, *Biomater. Sci.* **2018**, *6*, 1424.
[14] M. Steglich, M. Zilk, A. Bingel, C. Patzig, T. Kasebier, F. Schrempel, E.-B. Kley, A. Tunnermann, *J. Appl. Phys.* **2013**, *114*, 183102.
[15] V. Torres-Costa, R. J. Martin-Palma, *J. Mater. Sci.* **2010**, *45*, 2823.
[16] A. S. Mayet, H. Cansizoglu, Y. Gao, S. Ghandiparsi, A. Kaya, C. Bartolo-Perez, B. AlHalaili, T. Yamada, E. P. Devine, A. F. Elrefaie, S.-Y. Wang, M. S. Islam, *J. Opt. Soc. Am. B* **2018**, *35*, 1059.
[17] J. H. Ahire, Q. Wang, P. R. Coxon, G. Malhotra, R. Brydson, R. Chen, Y. Chao, *ACS Appl. Mater. Interfaces* **2012**, *4*, 3285.
[18] X. G. Zhang, *J. Electrochem. Soc.* **2004**, *151*, C69.
[19] J. Müllerová, L. Scholtz, J. Ďurišová, E. Pinčík, M. Solanská, D. Pudiš, *Appl. Surf. Sci.* **2018**, *461*, 182.
[20] R. Bilyalov, L. Stalmans, J. Poortmans, *J. Electrochem. Soc.* **2003**, *150*, G216.
[21] M. Alaya, R. B. Zaghouani, S. Khamlich, J.-L. Lazzari, W. Dimassi, *Thin Solid Films* **2018**, *645*, 51.
[22] Y. Liu, T. Lai, H. Li, Y. Wang, Z. Mei, H. Liang, Z. Li, F. Zhang, W. Wang, A. Y. Kuznetsov, X. Du, *Small* **2012**, *8*, 1392.
[23] F. Toor, J. B. Miller, L. M. Davidson, L. Nichols, W. Duan, M. P. Jura, J. Yim, J. Forziati, M. R. Black, *Nanotechnology* **2016**, *27*, 412003.
[24] F. Es, G. Baytemir, M. Kulakci, R. Turan, *Sol. Energy Mater. Sol. Cells* **2017**, *160*, 269.
[25] J. Oh, H.-C. Yuan, H. M. Branz, *Nat. Nanotechnol.* **2012**, *7*, 743.
[26] G. Su, R. Jia, X. Dai, K. Tao, H. Sun, Z. Jin, X. Liu, *IEEE J. Photovoltaics* **2018**, *8*, 937.
[27] S. Koynov, M. S. Brandt, M. Stutzmann, *Appl. Phys. Lett.* **2006**, *88*, 203107.
[28] S. Koynov, M. S. Brandt, M. Stutzmann, *J. Appl. Phys.* **2011**, *110*, 043537.
[29] P. Repo, J. Benick, V. Vahanissi, J. Schon, G. V. Gastrow, B. Steinhauser, M. C. Schubert, M. Hermle, H. Savin, *Energy Procedia* **2013**, *38*, 866.
[30] H. V. Jansen, M. J. D. Boer, S. Unnikrishnan, M. C. Louwerse, M. C. Elwenspoek, *J. Micromech. Microeng.* **2009**, *19*, 033001.
[31] C. Modanese, S. H. Laine, P. T. Pasanen, H. Savin, M. J. Pearce, *Energies* **2018**, *11*, 2337.
[32] L. Sainiemi, V. Jokinen, A. Shah, M. Shpak, S. Aura, P. Suvanto, S. Franssila, *Adv. Mater.* **2011**, *23*, 122.
[33] A. Ingenito, O. Isabella, M. Zeman, *Prog. Photovoltaics: Res. Appl.* **2015**, *23*, 1649.
[34] H. Savin, P. Repo, G. V. Gastrow, P. Ortega, E. Calle, M. Garin, R. Alcubilla, *Nat. Nanotechnol.* **2015**, *10*, 624.
[35] J. Benick, R. Müller, F. Schindler, A. Richter, H. Hauser, F. Feldmann, P. Krenckel, S. Riepe, M. C. Schubert, M. Hermle, S. W. Glunz, in *Proc. of 33rd European Photovoltaic Solar Energy Conf. and Exhibition (EU PVSEC 2017, Amsterdam)*, WIP Wirtschaft und Infrastruktur GmbH & Co Planungs-KG, Munich **2017**.
[36] P. Repo, A. Haarahiltunen, L. Sainiemi, M. Yli-Koski, H. Talvitie, M. C. Schubert, H. Savin, *IEEE J. Photovoltaics* **2013**, *3*, 90.
[37] A. Ingenito, O. Isabella, M. Zeman, *ACS Photonics* **2014**, *1*, 270.
[38] M. M. Plakhotnyuk, M. Gaudig, J R. S. Davidsen, M. Lindhard, J. Hirsch, D. Lausch, M. S. Schmidt, E. Stamate, O. Hansen, *J. Appl. Phys.* **2017**, *122*, 14.
[39] J. Yoo, G. Yu, J. Yi, *Mater. Sci. Eng. B* **2009**, *90*, 3085.
[40] B. Liu, S. Zhong, J. Liu, Y. Xia, C. Li, *Int. J. Photoenergy* **2012**, *2012*, 971093.
[41] J. S. Yoo, I. O. Parm, U. Gangopadhyay, K. Kim, S. K. Dhungel, D. Mangalaraj, J. Yi, *Sol. Energy Mater. Sol. Cells* **2006**, *90*, 3085.
[42] W. F. Liu, J. M. Bian, Z. C. Zhao, Y. L. Luo, Z. Yuan, B. Y. Zhang, A. M. Liu, *ECS Solid State Lett.* **2013**, *2*, Q17.
[43] M. Otto, M. Kroll, T. KSsebier, R. Salzer, R. B. Wehrspohn, *Energy Procedia* **2012**, *27*, 361.
[44] W.-C. Wang, C.-W. Lin, H.-J. Chen, C.-W. Chang, J.-J. Huang, M.-J. Yang, B. Tjahjono, J.-J. Huang, W.-C. Hsu, M.-J. Chen, *ACS Appl. Mater. Interfaces* **2013**, *5*, 9752.
[45] T. Pasanen, V. Vahanissi, N. Theut, H. Savin, *Energy Procedia* **2017**, *124*, 307.
[46] B. W. H. Van De Loo, A. Ingenito, M. A. Verheijen, O. Isabella, M. Zeman, W. M. M. Kessels, *Appl. Phys. Lett.* **2017**, *110*, 263106.
[47] M. Mews, C. Leendertz, M. Algasinger, S. Koynov, L. Korte, *Phys. Status Solidi RRL* **2014**, *8*, 831.
[48] B. Iandolo, M. Plakhotnyuk, R. S. Davidsen, E. Stamate, O. Hansen, S. Nunomura, presented at *7th World Conf. on Photovoltaic Energy Conversion, WCPEC-7*, IEEE, Hawaii, June **2018**.
[49] R. Khandelwal, U. Plachetka, B. Min, C. Moormann, H. Kurz, *Microelectron. Eng.* **2013**, *111*, 220.
[50] M. Otto, M. Kroll, T. Kasebier, R. Salzer, A. Tunnermann, R. B. Wehrspohn, *Appl. Phys. Lett.* **2012**, *100*, 191603.
[51] Y. Yu, Z. Zhang, X. Yin, A. Kvit, Q. Liao, Z. Kang, X. Yan, Y. Zhang, X. Wang, *Nat. Energy* **2017**, *2*, 17045.
[52] W.-C. Wang, M.-C. Tsai, J. Yang, C. Hsu, M.-J. Chen, *ACS Appl. Mater. Interfaces* **2015**, *7*, 10228.
[53] J. Cui, S. P. Phang, H. C. Sio, Y. Wan, Y. Chen, P. Verlinden, A. Cuevas, *Phys. Status Solidi RRL* **2017**, *11*, 1700296.
[54] A. Paduthol, M. K. Juhl, G. Nogay, P. Löper, T. Trupke, *Prog. Photovoltaics: Res. Appl.* **2018**, *26*, 968.
[55] O. Levenspiel, *Chemical Reaction Engineering*, 3rd ed., John Wiley & Sons, New York **1999**.
[56] C. Shin, J. Park, S. Kim, J. Jang, J. Jung, Y.-J. Lee, J. Yi, *J. Nanosci. Nanotechnol.* **2014**, *14*, 10.

[57] C. Shin, S. M. Iftiquar, J. Park, Y. Kim, S. Baek, J. Jang, M. Kim, J. Jung, Y. Lee, S. Kim, J. Yi, *Thin Solid Films* **2013**, *547*, 256.
[58] M. S. Valipa, E. S. Aydil, D. Maroudas, *Surf. Sci.* **2004**, *572*, L339.
[59] W. M. M. Kessels, A. H. M. Smets, D. C. Marra, E. S. Aydil, D. C. Schram, M. C. M. V. D. Sanden, *Thin Solid Films* **2001**, *383*, 154.
[60] M. Z. Burrows, U. K. Das, R. L. Opila, S. De Wolf, R. W. Birkmire, *J. Vac. Sci. Technol. A* **2008**, *26*, 683.
[61] S.-K. Kim, J. C. Lee, S.-J. Park, Y.-J. Kim, K. H. Yoon, *Sol. Energy Mater. Sol. Cells* **2008**, *92*, 298.
[62] J.-C. Hsiao, C.-H. Chen, D.-C. Wu, P. Yu, *ECS Solid State Lett.* **2014**, *3*, P33.
[63] J. Ge, Z. P. Ling, J. Wong, T. Mueller, A. G. Aberle, *Energy Procedia* **2012**, *15*, 107.
[64] D. Deligiannis, R. Vasudevan, A. H. M. Smets, R. A. C. M. M. van Swaaij, M. Zeman, *AIP Adv.* **2015**, *5*, 097165.
[65] H. Meddeb, T. Bearda, Y. Abdelraheem, H. Ezzaouia, I. Gordon, J. Szlufcik, J. Poortmans, *J. Phys. D: Appl. Phys.* **2015**, *48*, 415301.
[66] S. De Wolf, M. Kondo, *Appl. Phys. Lett.* **2007**, *90*, 042111.
[67] D. Deligiannis, S. Alivizatos, A. Ingenito, D. Zhang, M. V. Sebille, R. A. C. M. M. van Swaaij, M. Zeman, *Energy Procedia* **2014**, *55*, 197.